Inorganic−Organic Coating via Molecular Layer Deposition Enables Long Life Sodium Metal Anode

Yang Zhao,[†] Lyudmila V. Goncharova,[‡] Qian Zhang,[§] Payam Kaghazchi,[§] Qian Sun,[†] Andrew Lushington,[†] Biqiong Wang,[†] Ruying Li,[†] and Xueliang Sun*,[†]

[†]Department of Mechanical and Materials Engineering, University of Western Ontario, London, Ontario N6A 5B9, Canada
[‡]Department of Physics and Astronomy, University of Western Ontario, London, Ontario N6A 3K7, Canada
[§]Physikalische und Theoretische Chemie, Freie Universität Berlin, D-14195 Berlin, Germany

S Supporting Information

ABSTRACT: Metallic Na anode is considered as a promising alternative candidate for Na ion batteries (NIBs) and Na metal batteries (NMBs) due to its high specific capacity, and low potential. However, the unstable solid electrolyte interphase layer caused by serious corrosion and reaction in electrolyte will lead to big challenges, including dendrite growth, low Coulombic efficiency and even safety issues. In this paper, we first demonstrate the inorganic−organic coating via advanced molecular layer deposition (alucone) as a protective layer for metallic Na anode. By protecting Na anode with controllable alucone layer, the dendrites and mossy Na formation have been effectively suppressed and the lifetime has been significantly improved. Moreover, the molecular layer deposition alucone coating shows better performances than the atomic layer deposition Al_2O_3 coating. The novel design of molecular layer deposition protected Na metal anode may bring in new opportunities to the realization of the next-generation high energy-density NIBs and NMBs.

KEYWORDS: Molecular layer deposition, alucone, metallic sodium anode, sodium protection
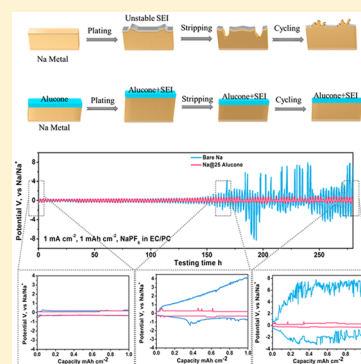
Na ion batteries (NIBs), room temperature Na−S and Na−O$_2$ batteries are highly attractive alternative candidates for future large-scale energy storage and conversion applications comparing with lithium ion batteries (LIBs) due to the wide availability and low cost of metallic sodium.[1−6] In particular, both room-temperature Na−S batteries and Na−O$_2$ batteries have very attractive theoretical specific energy density of 1274 and 1605 Wh kg^{-1}, respectively.[7−9] Similar to Li metal anode in LIBs, the reaction between metallic Na and commonly employed liquid electrolytes leads to the formation of a solid electrolyte interphase (SEI) on the surface of Na. However, the SEI layer formed in Na carbonate electrolytes is relatively unstable, which leads to nonuniform ionic flux during repetitive Na stripping/plating process as well as low columbic efficiency (CE) and may result in the growth of mossy or dendritic Na causing significant safety issues (Figure 1). As indicated in the previous references,[10,11] a number of challenges are still needed to be addressed for the use of metallic Na as an anode in sodium based batteries. Cui's group reported the obvious dendrite growth, short lifetime, and low CEs of NaPF$_6$ in carbonate-based electrolyte (EC/DEC, EC/DMC), which is in contrast to the significantly improved CEs and dendrite free Na growth in NaPF$_6$-glyme-based electrolyte that can be attributed to the formation of a compact SEI comprised of Na$_2$O and NaF in the ether-based electrolyte.[12]

The use of different coatings to suppress the side reactions and dendrite growth can be another very effective approach for Li and Na anodes. Atomic layer deposition (ALD) possesses the unique advantages of providing an excellent coverage, conformal depositions, and highly controllable thicknesses.[13,14] ALD has been widely studied as a novel coating technique for cathode/anode electrodes in LIBs to prevent the side reactions because of the direct contact of the electrode with the electrolyte and contribute to form a stable SEI layer, which is important to achieve improved electrochemical performances.[15−18] Recent research has revealed that ALD Al$_2$O$_3$-coated Li metal can successfully prevent electrolyte corrosion of the anode as well as minimize Li dendritic growth, thereby enhancing electrochemical performance.[19,20] As for Na anode, our group and Hu's group have successfully demonstrated that the use of ALD Al$_2$O$_3$ coating can also improve the stability of Na anode during stripping/plating, prolong its cycling lifetime, and suppress dendrite growth in ether and carbonate solvent electrolyte systems, respectively.[21,22]

In comparison to inorganic coatings, organic coatings or inorganic−organic hybrid coatings may be expected to enable further improved performance of the electrode with huge volume change. Molecular layer deposition (MLD), as an analogue of ALD, can be employed to produce inorganic−organic hybrid or pure polymer thin films with many
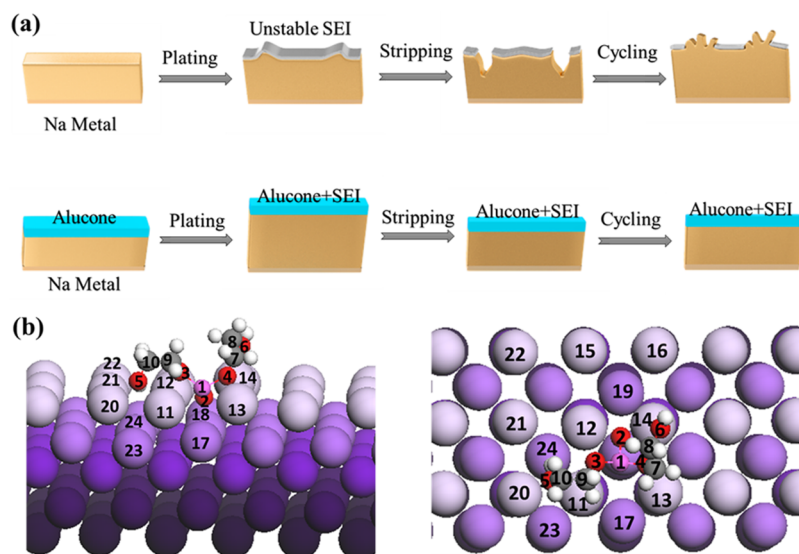
Figure 1. (a) Schematic diagrams of Na stripping/plating on bare Na foil and Na foil with MLD alucone coating; (b) 3D and top views of adsorption of a single alucone molecule on the Na(100) surface. The calculated Bader charges for labeled atoms are listed in Table S1.

advantages such as tunable thermal stability and improved mechanical properties.[23,24] In a typical MLD process, the oxidizing precursor in ALD (like H_2O, O_2, and so forth) can be replaced with organic linkers or added to a molecular fragment into the film. For instance, Ban et al. employed the use of an MLD alucone layer (a hybrid film produced through a reaction between trimethylaluminum and glycerol (Al-GL)) as a surface modifier for conventional nano-Si composites, providing significant improvement to cycling stability, rate, and CE, which can be attributed to the increased toughness and flexibility as a result of C—C and C—O bonds within the alucone film, thereby providing ample room for the huge volume expansion observed for Si anodes.[25−27] Our group has also demonstrated the use of MLD alucone as a coating material to improve the electrochemical performance of carbon/sulfur cathode electrode in Li−S batteries.[28,29] Therefore, the merits of MLD thin film coating can be also expected to relieve the volume expansion and suppress the dendrite growth for Na anode.

Herein, we demonstrate for the first time the application of MLD alucone as a protecting layer for Na metal anode cycled in carbonate-based electrolyte ($NaPF_6$ in EC/PC). Compared to bare Na and ALD Al_2O_3-coated Na, MLD-coated Na shows significantly enhanced electrochemical stripping/plating performances under various current densities, results in the formation of a smooth Na surface following plating and stripping, and can effectively reduce the formation of Na dendrites. Also, we should mention that we carried out mechanistic study by X-ray photoemission (XPS) and Rutherford Backscattering Spectroscopies (RBS).

The MLD alucone thin film was deposited on fresh Na metal using sequential exposures of trimethylaluminum (TMA) and ethylene glycol (EG) at 85 °C in a glovebox-integrated ALD tool. A typical MLD process of alucone deposition has been verified recording the mass gain per MLD cycle via in situ quartz crystal microbalance (QCM) sensor measurements at 85 °C (shown in Figure S1). The mass gain maintains a constant value ($\Delta \sim 60$ ng cm^{-2}) from cycle to cycle for both TMA and EG at 85 °C, which is similar to the reported value in the literature (Figure S1b). To confirm the uniform and conformal

nature of the alucone MLD process, 100cy of deposition was conducted on nitrogen-doped carbon nanotubes, as shown in Figure S2. To investigate the influence of alucone film's thickness on the electrochemical plating and stripping of Na anode, 10, 25, and 40 MLD cycle coatings were conducted and named as Na@10Alucone, Na@25Alucone, Na@40Alucone, respectively. X-ray photoelectron spectroscopy (XPS) was used to detect the surface composition of MLD coated Na (Figure S3a), confirming the presence of Al, C, and O. The C 1s XPS spectra of Na@25Alucone is shown in Figure S3c, in which the peak at 285 eV is attributed to adventitious C—H species and peak at 286.5 eV is attributed to C—O species, respectively. Meanwhile, the O 1s spectra and Al 2p spectra are shown in Figure S3b,d, which are very similar to the peaks in Al_2O_3 films. It can be concluded that the MLD alucone coating containing Al and EG has been successfully deposited on Na foil. For comparison, Na coated with ALD Al_2O_3 has been also fabricated.

To confirm the strong interaction between the protecting alucone layer with the surface of Na, we have studied structure, energetics, and Bader charges for adsorption of an alucone molecule on Na(100) using density functional theory (DFT) and ab initio molecular dynamics (AIMD) calculations. We chose the Na(100) surface because an ab initio thermodynamics study on Li shows that (100) has the highest contribution among the low-index facets to the particle of Li.[30] To determine the most favorable structure, we have first performed DFT calculations for adsorption of alucone from its O_2 side (see Figure 1b) to four possible different binding sites (top, short-bridge, long-bridge, and 4-fold hollow) on the surface. Afterward, we have performed AIMD-NVT simulations for 11 ps at 600 K for the DFT-determined minimum energy structure (4-fold hollow site). Finally, we have carried out a DFT calculation for the final structure of the AIMD simulation. The structure that was determined in this way (see Figure 1b) is 0.73 eV more favorable than that was obtained in the DFT calculation before the AIMD simulation. As can be seen in Figure 1b, the molecule adsorbs parallel to the surface so that Al and O atoms can interact with Na surface atoms. Hence, the calculated adsorption energy of 5.50 eV for alucone/Na(100) is
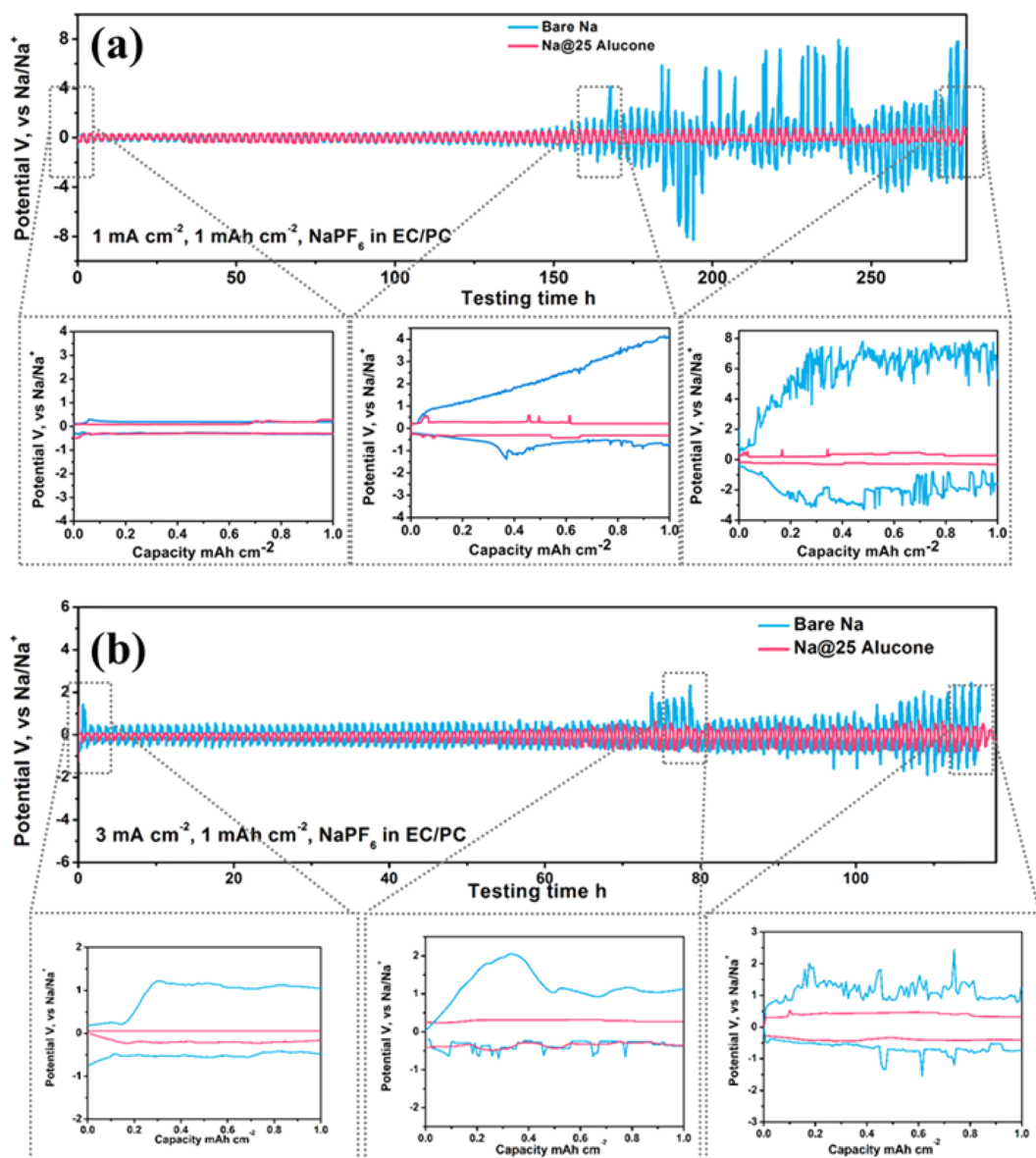
Figure 2. (a) Comparison of the cycling stability of the Na@25alucone and the bare Na foil at a current density of 1 mA cm^{-2}; potential profiles of Na@25alucone and bare Na foil at the three different stages. (b) Comparison of the cycling stability of the Na@25alucone and the bare Na foil at a current density of 3 mA cm^{-2}; potential profiles of Na@25alucone and bare Na foil at three different stages. The amount of Na cycled was 1 mAh cm^{-2}.

very strong. Afterward, we analyzed the Bader charges (see Table S1). A total electron transfer of 2.87 |e| from the surface to the molecule is found, confirming the strong adsorption energy. Table S1 indicates that the main electron transfer from the surface is toward Al and O2. There are also small electron transfers from Na(100) to other O atoms (0.14 |e| − 0.24 |e|). Therefore, the strong interaction between alucone and Na is due to the O—Na and Al—Na bonds.

Galvanostatic cycling of MLD alucone-coated Na and bare Na foil was studied using a symmetrical cell configuration (MLD coated) Na/carbonate electrolyte plus separator/(MLD coated) Na, using the electrolyte of 1 M NaPF$_6$ dissolved in 1:1 (v/v) EC/PC. Figure 2a presents a comparison of the cycling stability of Na@25alucone and bare Na foil at a current density of 1 mA cm^{-2} with a capacity limitation of 1 mAh cm^{-2}. For bare Na foil, an initial stripping/plating overpotential of about 200 mV (versus Na$^+$/Na) is observed. The subsequent

overpotentials gradually increase to over 4000 mV (versus Na$^+$/Na) after about 160 h. Furthermore, rapid uncontrolled fluctuations of the plating/stripping curves can be observed with soft short circuiting of the cell occurring after 160 h. Interestingly, Na@25alucone demonstrates a similar initial overpotential of about 200 mV (versus Na$^+$/Na) but demonstrates negligible change in the overpotential over the following 270 h (300 mV versus Na$^+$/Na). Detailed potential profiles of Na@25alucone and bare Na foil at a current density of 1 mA cm^{-2} at three different stages are shown in Figure 2a. For Na@25alucone, a virtually flat voltage plateau is observed during both charging and discharging states and is retained throughout the cycle life with negligible increase in hysteresis. However, the bare Na displays a significant increase as well as unstable overcharging potential after 160 and 270 h. When increasing the current density up to 3 mA cm^{-2}, the bare Na foil shows a larger overpotential than Na@25alucone during
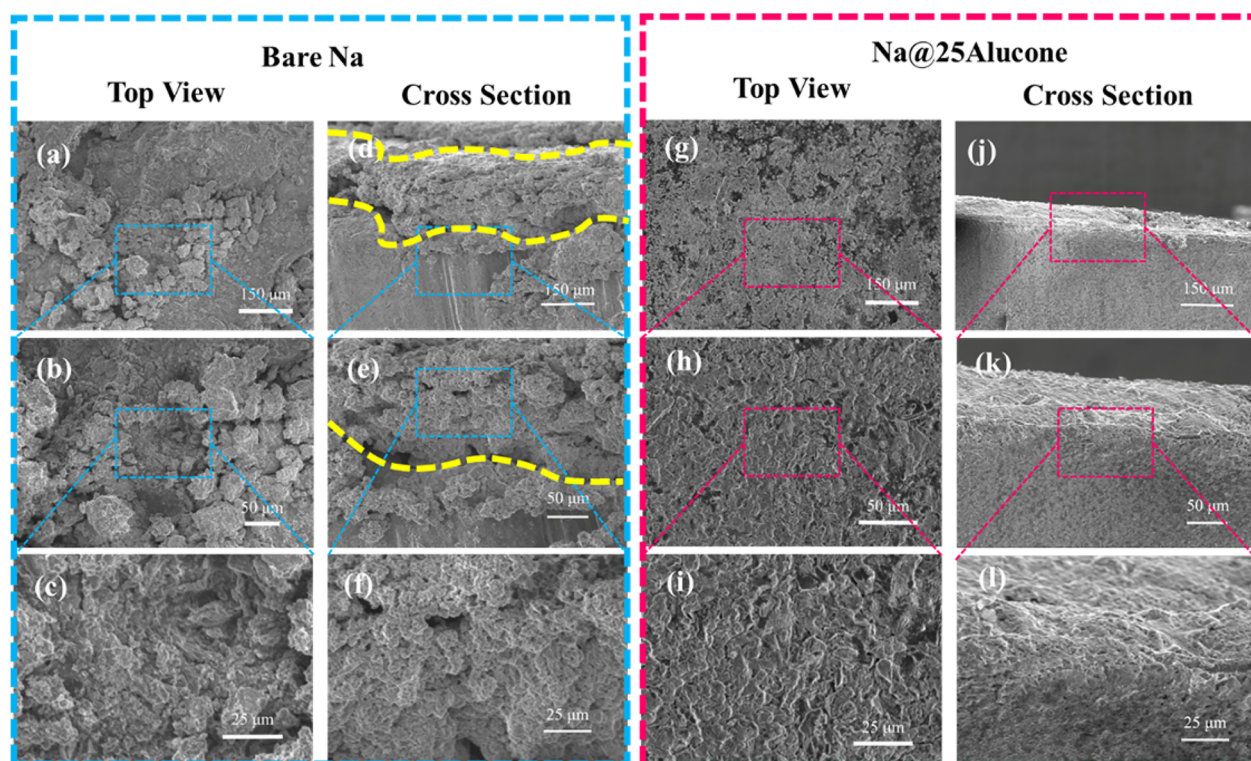
Figure 3. Top-view and cross section view SEM images of bare Na (a−f) and Na@25Alucone (g−l) after 10 cycles of stripping/plating at a current density of 1 mA cm^{-2} with the capacity of 1 mAh cm^{-2}.
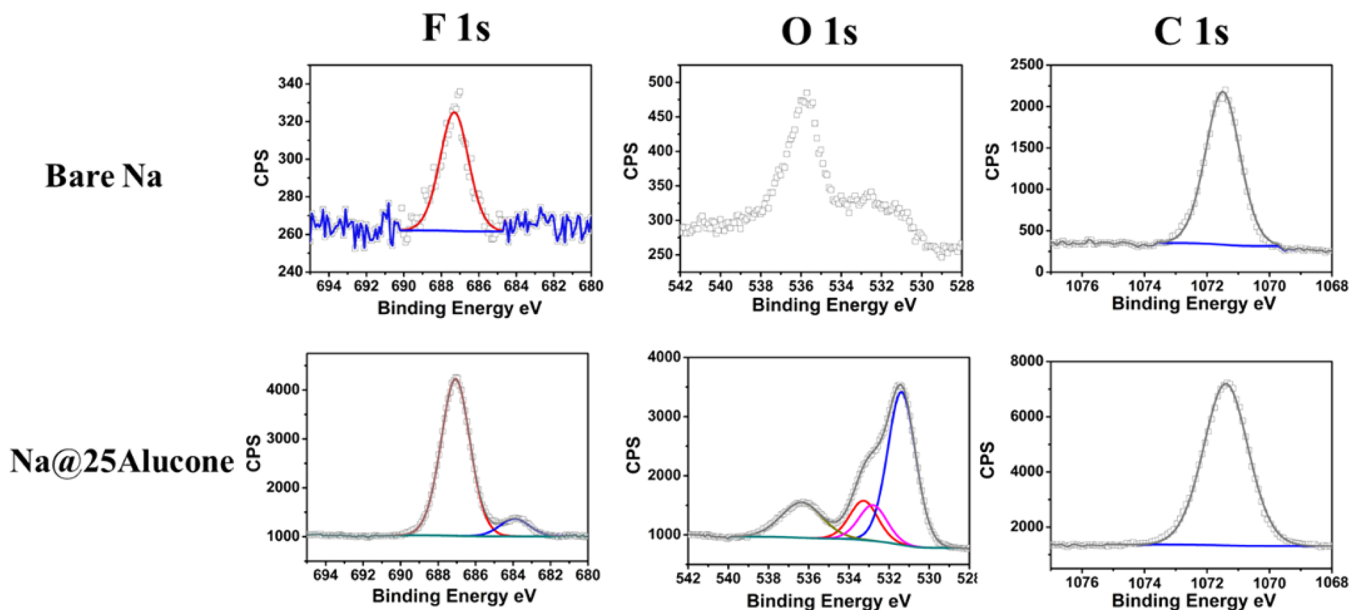

Figure 4. XPS F 1s, O 1s, and Na 1s spectrum of bare Na and Na@25alucone after 10 cycles of plating/stripping at the current density of 1 mA cm^{-2}.

initial cycle and starts to increase after 80 h (Figure 2b). Meanwhile, the overpotential of bare Na foil rises up to over 1500 mV after 100 h. However, Na@25alucone demonstrates reduced lower initial overpotential (200 mV versus Na$^+$/Na), which is extremely stable after 100 h with the overpotential of 400 mV (versus Na$^+$/Na). A similar phenomenon can be observed from the voltage plateau in the three different stages at the current density of 3 mA cm^{-2}. The voltage hysteresis

gradually increase in the cells made with bare Na metal and ultimately fails after 80 h.

To find the optimized MLD alucone thickness, various cycle numbers of alucone MLD (10 and 40 cycles) were performed on Na. Figure S4 and Figure S5 display the electrochemical plating/stripping performances and potential profiles of Na@ 10alucone at a current density of 1 and 3 mA cm^{-2}. The results indicate that a thinner MLD coating of 10 alucone cycles can also prevent an increase in overpotential with prolonged cycling
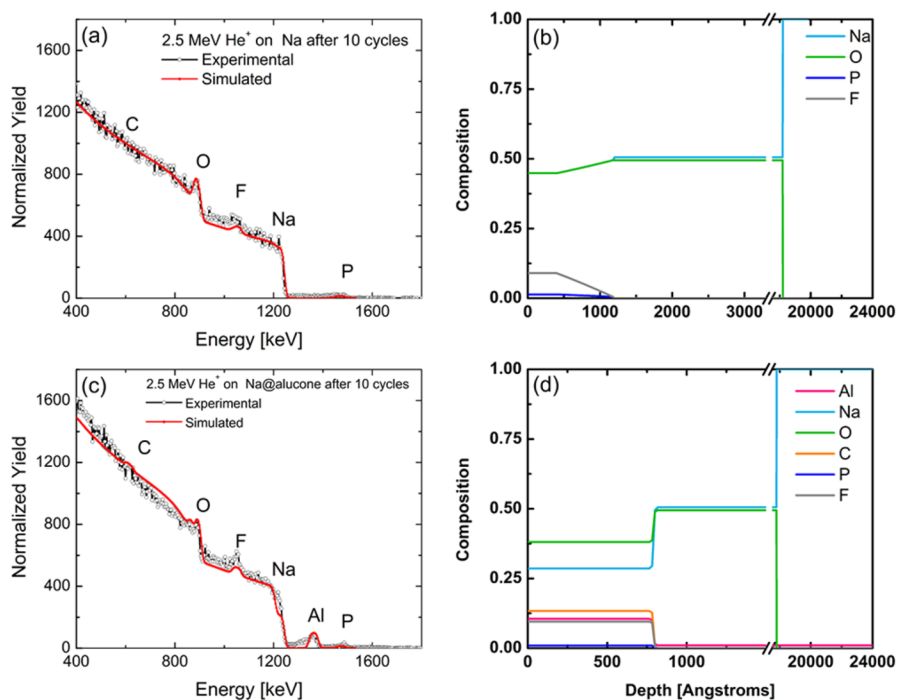
Figure 5. RBS spectra and calculated depth profiles for bare Na (a,b) and Na@25alucone (c,d) after 10 cycles plating/stripping.

and contributes toward preventing mossy and dendritic growth but cannot retain as good prolonged performances as Na@25alucone. Similarly, results can be obtained with a thicker coating of 40 cycles of MLD alucone. Although enhanced stability can be achieved, the modified Na foil with 40 cycles of alucone coating consistently demonstrates elevated overpotential and increasing hysteresis compared with 25 cycles MLD alucone coating (Figure S6).

In order to understand the improved performance of MLD alucone-coated Na electrode compared to bare Na, the morphologies of bare Na and Na@25alucone before and after cycling were analyzed by SEM. Figure 3 compares the SEM images of bare Na and Na@25alucone after 10 cycles of electrochemical plating/stripping at a current density of 1 mA cm^{-2} with the capacity limit of 1 mAh cm^{-2}. From top view SEM images (Figure 3a–c), moss-like and 3D sphere-like structures of Na dendrites of the thickness of approximately 10 μm can be clearly observed for bare Na. Furthermore, following electrochemical cycling, the surface of Na metal appears to have increased surface roughness as well as high surface area comprising of porous SEI material (Figure S7). Cross-sectional SEM images of cycled bare Na have also been investigated and are displayed in Figure 3d–f. From Figure 3d, a clear distinction between Na dendrite growth and subsurface bulk Na can be seen in which the Na dendrite layer is approximately 150 μm. The high surface area Na dendrite can also be observed in Figure 3e,f. These types of moss/dendritic Na will further lead to the formation of dead sodium during the plating/stripping process, which will consume effective Na and decrease CE. Interestingly, through the use of an alucone coating, the surface morphology of electrochemically cycled Na is relativity smoothed and does not have any high surface area moss/dendritic Na, as shown in Figure 3g–i and Figure S7. Meanwhile, the cross-section view of Na@25alucone (Figure 3i–l) displays a negligible gap between plated Na and bulk Na, indicating uniform electrochemical deposition of Na. It can be

certified that with an alucone layer, the Na dendrite can be effectively reduced to form a smooth surface on Na metal, which can play an important role in the improved electrochemical performance.

XPS testing was employed to determine the surface chemical nature of bare Na and Na@25alucone electrodes after 10 cycles of electrochemical plating and stripping. The F 1s, O 1s, and Na 1s XPS spectra of each sample are shown in Figure 4. In the F 1s spectrum, the peak at 686 eV occurs in both samples, which is due to residual Na$_x$PF$_y$ and Na$_x$PO$_y$F$_z$ on the surface. However, an extra F peak of 683 eV can be observed from Na@25alucone after cycling, which can be assigned as the Na–F (NaF) peak. For the O 1s spectra, there are no obvious O peaks in the bare Na after cycling, however, the O 1s peak of 530.9 eV in Na@25alucone after cycling is the formation of Na$_2$O-like phase in the SEI layers. Meanwhile, the content of F, O and Na in bare Na sample is much less than that in the Na@25alucone indicating unstable SEI formation on bare Na. This causes additional Na to be exposed to electrolyte, resulting in undesirable side reactions, consuming both active Na and electrolyte thus, and lowering the columbic efficiency of the cell. Furthermore, the nonuniformity of the SEI results in nonuniform Na$^+$ flux and dendritic growth of Na metal, causing constant breaking and reforming of the SEI.[12] However, the SEI in Na@25alucone mainly consist Na–O (530.9 eV) and Na–F (683.9 eV), which is considered as stable SEI components and highly impermeable to the electrolyte solvent, resulting in uniform Na$^+$ flux and reduced dendrite growth of Na metal.[12]

Rutherford backscattering spectrometry (RBS) measurements were performed on bare Na and Na@25alucone electrodes before and after 10 plating/stripping cycles to confirm film thicknesses and deduce elemental depth profiles. Figure S10 show RBS spectrum for alucone-coated Na foil before electrochemical plating/stripping and calculated depth profiles. As evident from sharp Al, C, and O surface peaks,

alucone layer ∼60 nm thick was developed on the Na surface after 25 MLD alucone cycles. Several samples with 25, 50, and 75 MLD deposition cycles were analyzed by RBS to determine alucone growth rate. Assuming a change in composition due to Na diffusion into alucone layer after deposition, the MLD growth rates of 0.62−1.0 nm/cycle were calculated, which are a factor of ∼20% higher compared to Li and a factor of ∼20% higher compared to the rate observed by SEM on nitrogen-doped carbon nanotubes and presented in Figure S2. It is considered that the higher growth rate of alucone on Na can be attributed to the reactions of Na and EG in the initial cycles leading to a thicker layer, which has also been observed and determined by Elam's group for ALD Al_2O_3 coating on Li.[31] Na profile goes all the way to the surface. In addition Al profile goes deeper (200−300 nm) into Na foil, consistent with morphological features observed in SEM and $Al(C_xO_y)$/Na interdiffusion. Remarkably Al peaks and associated depth profiles do not change dramatically after 10 cycles of stripping/plating (Figure 5). P and F contents are higher in SEI layer for alucone covered Na compared to a bare Na sample, after electrochemical cycling, which is also consistent with XPS results presented above. P and F from $NaPF_6$ penetrate well into $Al(C_xO_y)$ layer and are likely to contribute to the overall stability of SEI. Notably, Na concentrations on the surface do not change significantly after electrochemical cycling, another argument toward enhanced stability of SEI in Na@alucone samples.

For comparison, 30 cycles of ALD Al_2O_3 was also been deposited on the surface of metallic Na, using TMA and water as precursors at 85 °C.[21] Figure S8 shows the electrochemical plating/stripping cycling performance of Na@$30Al_2O_3$ under a current density of 1 and 3 mA cm^{-2}. It can be found that the lifetime of Na@$30Al_2O_3$ can be partially enhanced compared to bare Na. However, the alucone-coated samples still outperforms ALD Al_2O_3. It is believed that the alucone coating is highly stable against liquid electrolyte and acts as a passivating agent to assist Na metal anode to form a stable SEI layer. Furthermore, an alucone coating is mechanically flexible[25] and allows for repeated Na plating/stripping on the surface of Na foil with significant roughness.

In conclusion, we demonstrate the first use of an inorganic−organic MLD-alucone protecting layer on metallic Na anode for long life Na metal batteries. By protecting Na foil with an ultrathin alucone layer, the formation of mossy and dendrite-like Na is effectively suppressed and lifetime significantly improved. Furthermore, a comparison between ALD Al_2O_3 and MLD alucone has also been investigated, demonstrating that the alucone-coated Na outperforms ALD Al_2O_3 by displaying prolonged lifetime and stable polarization curves. It is believed that our design of alucone-coated metal Na anode opens up new opportunities to the realization of next-generation high energy density Na metal batteries.

■ ASSOCIATED CONTENT

ⓢ Supporting Information

The Supporting Information is available free of charge on the ACS Publications website at DOI: 10.1021/acs.nano-lett.7b02464.

Additional information and figures (PDF)

■ AUTHOR INFORMATION

Corresponding Author

*E-mail: xsun@eng.uwo.ca (X.L.S.).

ORCID

Yang Zhao: 0000-0002-4148-2603
Xueliang Sun: 0000-0003-2881-8237

Notes

The authors declare no competing financial interest.

■ REFERENCES

(1) Zhao, Y.; Li, X. F.; Yan, B.; Xiong, D. B.; Li, D. J.; Lawes, S.; Sun, X. *Adv. Energy. Mater.* **2016**, *6*, 1502175.
(2) Zhao, Y.; Song, Z.; Li, X.; Sun, Q.; Cheng, N.; Lawes, S.; Sun, X. *Energy Storage Mater.* **2016**, *2*, 35−62.
(3) Zhao, Y.; Li, X.; Yan, B.; Li, D.; Lawes, S.; Sun, X. *J. Power Sources* **2015**, *274*, 869−884.
(4) Xia, C.; Fernandes, R.; Cho, F. H.; Sudhakar, N.; Buonacorsi, B.; Walker, S.; Xu, M.; Baugh, J.; Nazar, L. F. *J. Am. Chem. Soc.* **2016**, *138*, 11219−11226.
(5) Sun, Q.; Yang, Y.; Fu, Z.-W. *Electrochem. Commun.* **2012**, *16*, 22−25.
(6) Sun, Q.; Yadegari, H.; Banis, M. N.; Liu, J.; Xiao, B.; Li, X.; Langford, C.; Li, R.; Sun, X. *J. Phys. Chem. C* **2015**, *119*, 13433−13441.
(7) Yadegari, H.; Norouzi Banis, M.; Lushington, A.; Sun, Q.; Li, R.; Sham, T.-K.; Sun, X. *Energy Environ. Sci.* **2017**, *10*, 286−295.
(8) Hartmann, P.; Bender, C. L.; Vracar, M.; Durr, A. K.; Garsuch, A.; Janek, J.; Adelhelm, P. *Nat. Mater.* **2012**, *12*, 228−232.
(9) Yadegari, H.; Li, Y.; Banis, M. N.; Li, X.; Wang, B.; Sun, Q.; Li, R.; Sham, T.-K.; Cui, X.; Sun, X. *Energy Environ. Sci.* **2014**, *7*, 3747−3757.
(10) Hartmann, P.; Bender, C. L.; Sann, J.; Durr, A. K.; Jansen, M.; Janek, J.; Adelhelm, P. *Phys. Chem. Chem. Phys.* **2013**, *15*, 11661−72.
(11) Zhao, N.; Li, C.; Guo, X. *Phys. Chem. Chem. Phys.* **2014**, *16*, 15646−52.
(12) Seh, Z. W.; Sun, J.; Sun, Y.; Cui, Y. *ACS Cent. Sci.* **2015**, *1*, 449−55.
(13) Meng, X.; Yang, X. Q.; Sun, X. *Adv. Mater.* **2012**, *24*, 3589−615.
(14) Meng, X. *Nanotechnology* **2015**, *26*, 020501.
(15) Wang, D.; Yang, J.; Liu, J.; Li, X.; Li, R.; Cai, M.; Sham, T.-K.; Sun, X. *J. Mater. Chem. A* **2014**, *2*, 2306.
(16) Li, X.; Liu, J.; Banis, M. N.; Lushington, A.; Li, R.; Cai, M.; Sun, X. *Energy Environ. Sci.* **2014**, *7*, 768−778.
(17) Xiao, B.; Liu, J.; Sun, Q.; Wang, B.; Banis, M. N.; Zhao, D.; Wang, Z.; Li, R.; Cui, X.; Sham, T. K.; Sun, X. *Adv. Sci.* **2015**, *2*, 1500022.
(18) Li, X.; Liu, J.; Meng, X.; Tang, Y.; Banis, M. N.; Yang, J.; Hu, Y.; Li, R.; Cai, M.; Sun, X. *J. Power Sources* **2014**, *247*, 57−69.
(19) Kazyak, E.; Wood, K. N.; Dasgupta, N. P. *Chem. Mater.* **2015**, *27*, 6457−6462.
(20) Kozen, A. C.; Lin, C.-F.; Pearse, A. J.; Schroeder, M. A.; Han, X.; Hu, L.; Lee, S.-B.; Rubloff, G. W.; Noked, M. *ACS Nano* **2015**, *9*, 5884−5892.
(21) Zhao, Y.; Goncharova, L. V.; Lushington, A.; Sun, Q.; Yadegari, H.; Wang, B.; Xiao, W.; Li, R.; Sun, X. *Adv. Mater.* **2017**, *29*, 1606663.
(22) Luo, W.; Lin, C.-F.; Zhao, O.; Noked, M.; Zhang, Y.; Rubloff, G. W.; Hu, L. *Adv. Energy. Mater.* **2017**, *7*, 1601526.
(23) Ban, C.; George, S. M. *Adv. Mater. Interfaces* **2016**, *3*, 1600762.
(24) Sundberg, P.; Karppinen, M. *Beilstein J. Nanotechnol.* **2014**, *5*, 1104−1136.

(25) Piper, D. M.; Travis, J. J.; Young, M.; Son, S. B.; Kim, S. C.; Oh, K. H.; George, S. M.; Ban, C.; Lee, S. H. *Adv. Mater.* **2014**, *26*, 1596–1601.

(26) Luo, L.; Yang, H.; Yan, P.; Travis, J. J.; Lee, Y.; Liu, N.; Piper, D. M.; Lee, S. H.; Zhao, P.; George, S. M.; Zhang, J. G.; Cui, Y.; Zhang, S.; Ban, C.; Wang, C. M. *ACS Nano* **2015**, *9*, 5559–5566.

(27) He, Y.; Piper, D. M.; Gu, M.; Travis, J.; George, S. M.; Lee, S. H.; Genc, A.; Pullan, L.; Liu, J.; Mao, S.; Zhang, J. G.; Ban, C.; Wang, C. M. *ACS Nano* **2014**, *8*, 11816–11823.

(28) Li, X.; Lushington, A.; Liu, J.; Li, R.; Sun, X. *Chem. Commun.* **2014**, *50* (68), 9757–60.

(29) Li, X.; Lushington, A.; Sun, Q.; Xiao, W.; Liu, J.; Wang, B.; Ye, Y.; Nie, K.; Hu, Y.; Xiao, Q.; Li, R.; Guo, J.; Sham, T. K.; Sun, X. *Nano Lett.* **2016**, *16*, 3545–9.

(30) Seriani, N. *Nanotechnology* **2009**, *20*, 445703.

(31) Chen, L.; Connell, J. G.; Nie, A. M.; Huang, Z. N.; Zavadil, K. R.; Klavetter, K. C.; Yuan, Y. F.; Sharifi-Asl, S.; Shahbazian-Yassar, R.; Libera, J. A.; Mane, A. U.; Elam, J. W. *J. Mater. Chem. A* **2017**, *5*, 12297–12309.